Spectrochimica Acta Part A: Molecular and Biomolecular Spectroscopy 136 (2015) 221–233

Contents lists available at ScienceDirect

Spectrochimica Acta Part A: Molecular and Biomolecular Spectroscopy

journal homepage: www.elsevier.com/locate/saa

Nuclear magnetic resonance, vibrational spectroscopic studies, physico-chemical properties and computational calculations on (nitrophenyl) octahydroquinolindiones by DFT method

M.A. Pasha [a,*], Aisha Siddekha [a,b], Soni Mishra [c], Sadeq Hamood Saleh Azzam [a], S. Umapathy [c]

[a] Department of Studies in Chemistry, Central College Campus, Bangalore University, Bangalore 560001, India
[b] Department of Chemistry, Smt. VHD Central Institute of Home Science, Bangalore 560001, India
[c] Department of Inorganic and Physical Chemistry, Indian Institute of Science, Bangalore 560012, India

HIGHLIGHTS

- The theoretical calculations were made using 6-311++G (d,p) method.
- Experimental IR and Raman spectra are in agreement with the theoretical results.
- Complete wave number assignments are performed on the basis of PED.
- Isotropic chemical shifts for ^{1}H and ^{13}C NMR were calculated using GIAO.
- Molecular electrostatic potential and thermodynamic functions have been investigated.

GRAPHICAL ABSTRACT

Comparison of the 2′-nitrophenyl and 3′-nitrophenyl isomers of octahydroquinolindiones.

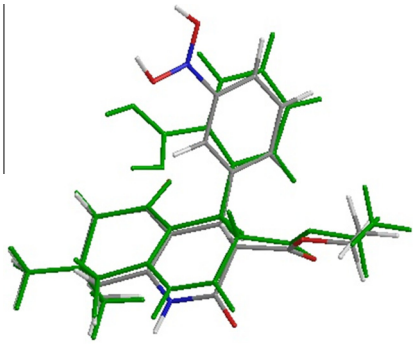

ARTICLE INFO

Article history:
Received 22 February 2013
Received in revised form 10 September 2014
Accepted 11 September 2014
Available online 5 October 2014

Keywords:
Octahydroquinolinediones
Raman spectroscopy
Vibrational spectroscopy
DFT
NMR
Computational studies

ABSTRACT

In the present study, 2′-nitrophenyloctahydroquinolinedione and its 3′-nitrophenyl isomer were synthesized and characterized by FT-IR, FT-Raman, ^{1}H NMR and ^{13}C NMR spectroscopy. The molecular geometry, vibrational frequencies, ^{1}H and ^{13}C NMR chemical shift values of the synthesized compounds in the ground state have been calculated by using the density functional theory (DFT) method with the 6-311++G (d,p) basis set and compared with the experimental data. The complete vibrational assignments of wave numbers were made on the basis of potential energy distribution using GAR2PED programme. Isotropic chemical shifts for ^{1}H and ^{13}C NMR were calculated using gauge-invariant atomic orbital (GIAO) method. The experimental vibrational frequencies, ^{1}H and ^{13}C NMR chemical shift values were found to be in good agreement with the theoretical values. On the basis of vibrational analysis, molecular electrostatic potential and the standard thermodynamic functions have been investigated.

Introduction

Quinolinones are naturally occurring compounds; they exhibit a broad spectrum of pharmacological activities which include anticancer [1], antihypertensive [2], antiviral [2], and antibiotic [3]

* Corresponding author. Tel.: +91 8022961337; fax: +91 8022961331.
E-mail address: m_af_pasha@ymail.com (M.A. Pasha).

http://dx.doi.org/10.1016/j.saa.2014.09.021
1386-1425/

activities. Toxicity of quinolinone is known to be low when compared to that of other commonly used antimicrobial agents; hence, quinolinones are considered to be relatively well-tolerated agents [4]. They are potent chemotherapeutic agents and are used for the development of inhibitors for the treatment of a broad range of bacterial infections [5]. Inhibitory activity of quinolinones against cathepsin V, a papain-like cysteine protease has been reported [6]. 2(1*H*)-Quinolinones have been reported to exhibit the cardiac stimulant activity [7] and methionyl-tRNA synthetase inhibition [8]. Quinolinone derivatives have also been patented for treating schizophrenia and related psychic disorders such as acute mania, bipolar disorder, autistic disorder and depression [9].

Literature survey reveals that, there are reports on the synthesis of quinolinones, but no structural study of such compounds seems to be present. Detailed knowledge on the molecular structure and spectral behavior of these compounds and their derivatives will aid the understanding of chemical and biological properties. In the present study, we describe the structural, vibrational, NMR and reactivity analyses of the derivatives of quinolinones *viz.*, 2′-nitrophenyloctahydroquinolindione (2′-NOHQ) and its isomer 3′-nitrophenyloctahydroquinolindione (3′-NOHQ) through spectral measurements. Theoretical calculations were carried out by density functional theory (B3LYP) method using 6-311++G (d,p) basis set. The calculated results were compared with the observed spectral values and were analyzed in detail. The aim of this work is to explore the molecular dynamics and the structural parameters which govern the chemical behavior, and to compare predictions made from the theory with the experimental observations.

Materials and methods

Synthesis

Occurrence of quinolinone scaffolds in a range of biologically active compounds, natural products and in the designed medicinal agents, necessitate the development of simple and efficient methods for the synthesis of quinolinones and their derivatives. Conventional methods of synthesis include the base-catalyzed Friedlander [10] and acid-catalyzed Knorr reactions [11]. Other reported methods are the Baylis–Hillman reaction [12], by the reduction of the nitro group into amino group using Zinc–Acetic acid followed by condensation sequence, and transition metal catalyzed cyclocarbonylation of 2-vinylanilines [13].

Reported methods are not completely satisfactory with regard to the yield, reaction conditions, cost of the reagents, catalysts, and due to involvement of multistep strategies.

Recently, we reported a multi-component synthesis of novel octahydroquinolindiones using ZnO as a readily available, inexpensive and environment friendly catalyst [14]. 2′-NOHQ and 3′-NOHQ were prepared by this method by refluxing a mixture of 2-nitrobenzaldehyde (1 mmol) or 3-nitrobenzaldehyde (1 mmol), diethyl malonate (1 mmol), ZnO (0.025 g, 7.5 mol%) in water (10 mL) for 30 min; dimedone (1 mmol) and ammonium acetate (2 mmol) were then added to the reaction mixture (Scheme 1) and refluxed for the remaining period (90 min). The crude product obtained was filtered and washed with water; the dry solid residue was treated with dichloromethane and filtered to get ZnO which could be reused. The filtrate was then evaporated to get the desired product, which was subjected to silica gel column chromatography [silica gel G, 100–200 mesh] to get the pure product in 90% yield. The structures of both the products were confirmed by their FT-IR, ^{1}H NMR, ^{13}C NMR spectral analyses.

Experimental details

FT-IR spectra were recorded in the range 4000–400 cm^{-1} on a Bruker Optics Alpha-P FT-IR spectrophotometer with attenuated total reflectance (ATR) module. The FT-Raman spectra were recorded in solid phase on Bruker Optics Multi-RAM FT-Raman spectrophotometer using Nd-YAG laser operating at 1064 nm as an excitation source at the resolution of 4 cm^{-1}. ^{1}H NMR and ^{13}C NMR spectra were obtained using a Bruker instrument operating at 400 MHz and 100 MHz respectively. Chemical shifts are reported on δ(delta) scale using tetra methyl silane as an internal standard and $CDCl_3$ as solvent. Elemental analysis was carried out using vario MICRO V1.9.7 elemental analyzer. All the reactions were monitored by thin-layer chromatography (TLC). All the chemicals and solvents used were commercial and of analytical grade.

Computational details

Calculations for electronic structure and geometry optimization of the stable isomers of the molecule were done by DFT [15] using the Gaussian 09 program [16] package employing 6-311++G (d,p) basis sets and Becke's three parameter (local, nonlocal, Hartree–Fock) hybrid exchange functionals with Lee–Yang–Parr correlation functionals (B3LYP) [17–19]. The absolute Raman intensities and infrared absorption intensities were calculated in the harmonic approximation at the same level of theory as used for the optimized geometries from the derivatives of the dipole moment and polarizability of each normal mode respectively. We have used hybrid DFT B3LYP 6-311++G (d,p) method for vibrational frequency calculations, which is known to be very appropriate; although GGA is found to be accurate method for predicting many material properties including vibrational properties, for example: Sarrio et al. [20] presented a comparative study between different DFT method for vibrational property calculations of triatomic molecules and concluded that GGA is more appropriate method than hybrid functional method, and recently very accurate GGA based calculations by Adjokatse et al. [21] also proved the accuracy of this method in case of polymeric systems.

The normal-mode analysis was employed to calculate PED for each of the internal coordinates using localized symmetry [22,23]. For this purpose a complete set of 144 internal coordinates was defined using Pulay's recommendations [22,23]. The vibrational assignments of the normal modes were proposed on the basis of the PED calculations using the program GAR2PED [24]. Raman and IR spectra were simulated using a pure Lorentzian band profile (fwhm = 10 cm^{-1}). Visualization and confirmation of the

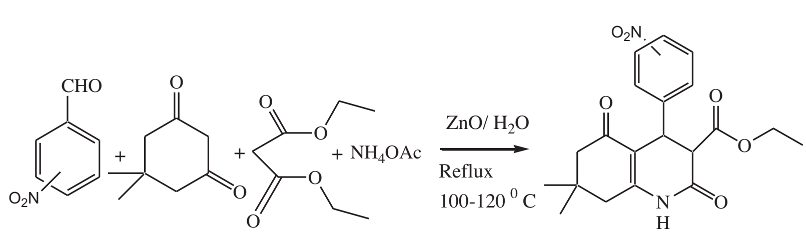

Scheme 1.

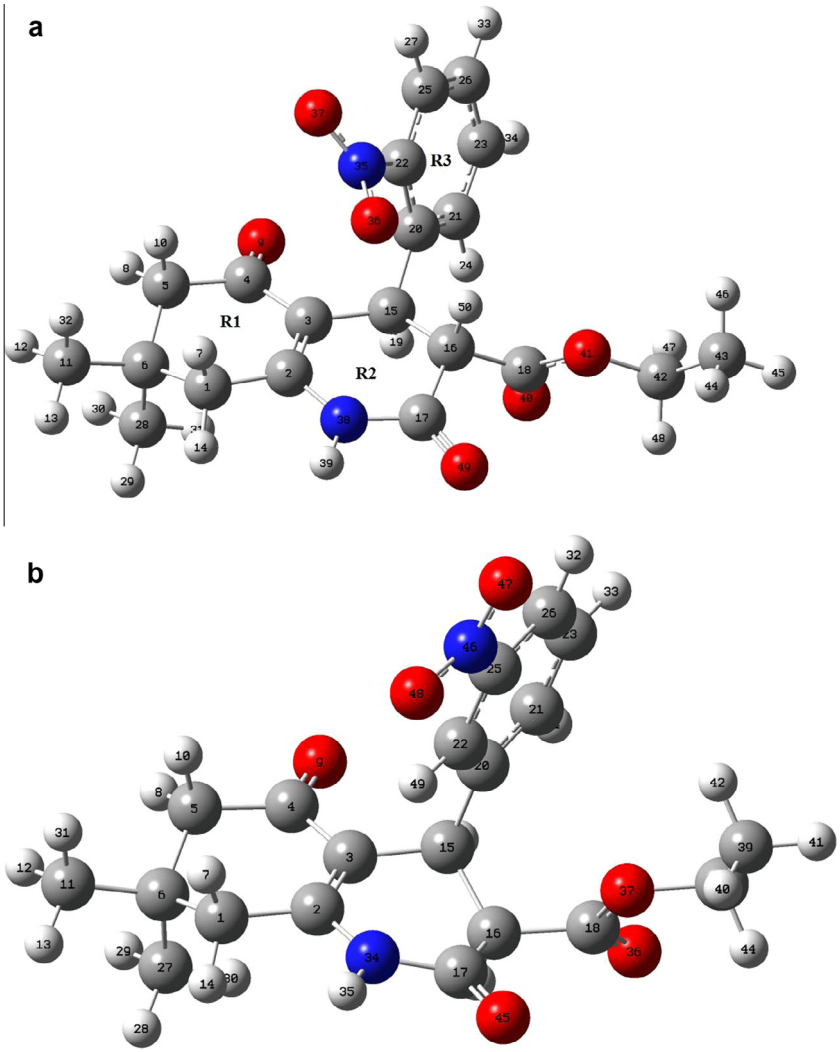

Fig. 1. Optimized structures of octahydroquinolindione isomers (a) 2′-NOHQ (b) 3′-NOHQ.

calculated forms of the vibrations were done using the CHEMCRAFT program [25].

Calculated DFT vibrational wave numbers are known to be higher than the experimental wave numbers as the anharmonicity effects are neglected. The vibrational wave numbers were obtained from the DFT calculations using a dual scaling procedure for the fingerprint region (below 1800 cm^{-1}) and X-H stretching (above 1800 cm^{-1}) regions respectively [26,27]. Recently, a few good papers using uniform scaling showed very good agreement between calculated and experimental frequencies [28]. In addition to uniform frequency scaling factors, dual scaling factors were determined to improve the agreement between computed and observed frequencies. The dual scaled error distributions are more symmetric, compared with the uniform scaled frequency errors [28]. All the calculated vibrational wavenumbers reported in this study are the scaled values.

Results and discussion

Molecular geometry

The molecular structures of both the isomers belong to C1 point group symmetry. The optimized molecular structures of the isomers were obtained from GAUSSIAN 09 program as shown in Fig. 1. The minimum energy of the title compound and its isomer was calculated to be −1336.539 by DFT method and −1336.546 by Hartree respectively. The enthalpy difference between these two molecules is 4.393 kcal/mol. Since these energy differences are much larger than *kT* (at room temperature), there is almost no possibility of coexistence of different molecules at room temperature.

The optimized structures of the 2′-NOHQ and 3′-NOHQ molecules were compared by superimposing them using a least-square algorithm which minimizes the distances between the corresponding non-hydrogen atoms (Fig. 2). The agreement between these molecules shows that, the geometry optimization almost reproduces the different conformations (overall average deviation 0.078 Å). The main differences are due to the position of the nitro group in the phenyl ring.

Molecular electrostatic potential

The molecular electrostatic potential (EPS) at a point *r* in the space around a molecule is (in atomic units):

$$V(r) = \sum_A \frac{ZA}{\left|\vec{R}A - \vec{r}\right|} - \int \frac{\rho(\vec{r}')dr'}{|\vec{r}' - \vec{r}|}$$

ZA is the charge on nucleus *A*, located at *RA* and $\rho(r')$ is the electronic density function for the molecule. The first term in the

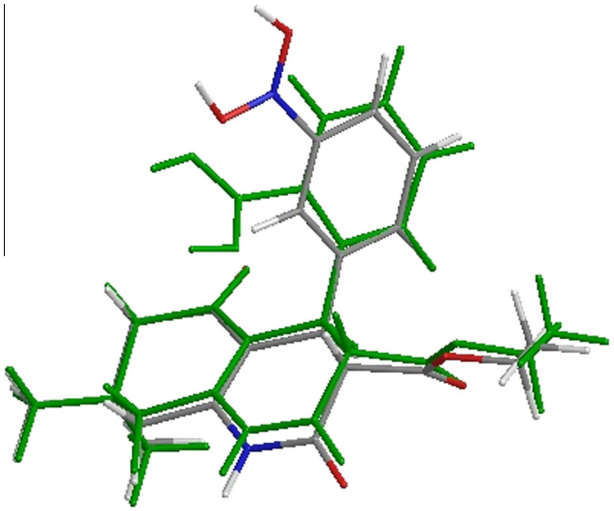

Fig. 2. Comparison of the 2′-nitrophenyl and 3′-nitrophenyl isomers of octahydroquinolindiones.

expression represents the effect of the nuclei; the second represents that of electrons. The two terms have opposite signs and therefore opposite effects. $V(r)$ is their resultant at each point r; it is an indication of the net electrostatic effect produced at the point r by the total charge distribution (electrons + nuclei) of the molecule. EPS serves as a useful quantity to explain hydrogen bonding, reactivity and structure–activity relationship of molecules [29].

Electrostatic potential correlates with dipole moment, electronegativity, partial charges and site of chemical reactivity of the molecule. It provides a visual method to understand the relative polarity of a molecule. While the negative electrostatic potential corresponds to an attraction of the proton by the concentrated electron density in the molecule, the positive electrostatic potential corresponds to repulsion of the proton by atomic nuclei in regions where low electron density exists and the nuclear charge is incompletely shielded. By definition, the electron density isosurface is a surface on which molecule's electron density has a particular value and that encloses a specified fraction of the molecule's electron probability density. Coloring the isosurface with contours shows the electrostatic potential at different points on the electron density isosurface. The electron density isosurface on to which the electrostatic potential surface has been mapped are shown in Figs. 3 and 4 for 2′-NOHQ and 3′-NOHQ respectively. The different values of the electrostatic potential at the surface are represented by different colors; red represents regions of most negative electrostatic potential, blue represents regions of most positive electrostatic potential and green represents regions of zero potential. Potential increases in the order red < orange < yellow < gre en < blue.

Vibrational analysis

The total number of atoms in the 2′-NOHQ molecule is 50 resulting in 144 (3*N*-6) normal modes. Here, *N* is the number of atoms in the molecule. The vibrational frequency and potential energy distribution of each normal modes obtained by DFT/B3LYP methods using 6-311++G (d,p) basis set for 2′-NOHQ and its isomer are summarized in Table 1. The title compound has the molecular formula of $C_{20}H_{22}O_6N_2$, belongs to C1 point group and has 144 normal modes of fundamental vibrations.

DFT calculations yield Raman scattering amplitudes which cannot be taken directly to be the Raman intensities. The Raman scattering cross section, $\partial\sigma_j/\partial\Omega$, which are proportional to Raman intensity may be calculated from the Raman scattering amplitude and predicted wavenumbers for each normal mode using the relationship [30,31].

$$\frac{\partial\sigma_j}{\partial\Omega} = \left(\frac{2^4\pi^4}{45}\right)\left(\frac{(v_0 - v_j)^4}{1 - \exp\left[\frac{-hcv_j}{kT}\right]}\right)\left(\frac{h}{8\pi^2 c v_j}\right)S_j$$

where S_j and v_j are the scattering activities and the predicted wavenumbers, respectively of the *j*th normal mode, v_0 is the wavenum-

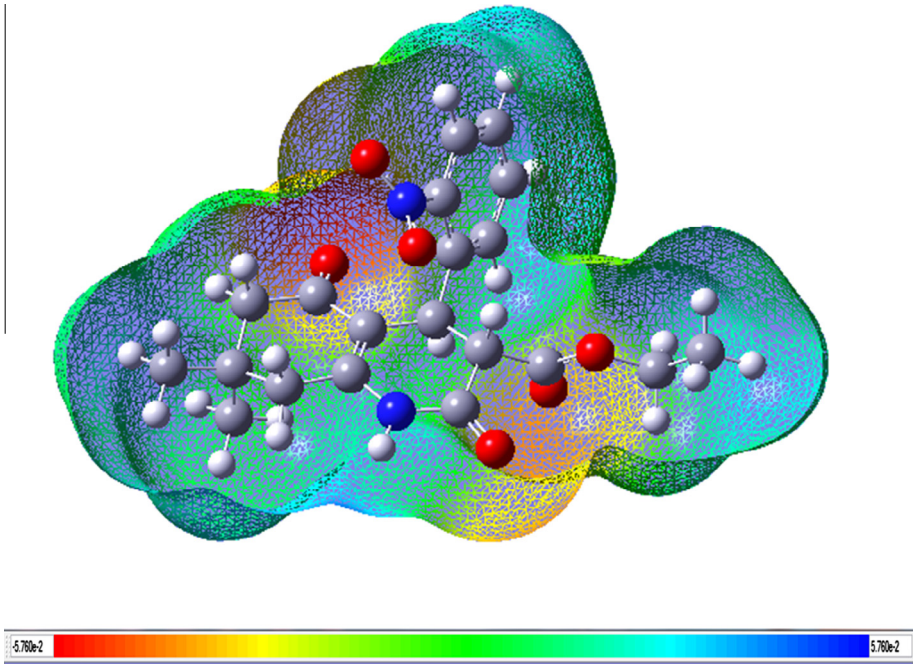

Fig. 3. Molecular electrostatic potential mapped on the isodensity surface in the range from −5.76e−2 (red) to +5.76e−2 (blue) for 2′-NOHQ calculated at the B3LYP/6-311G (d,p) level of theory. (For interpretation of the references to color in this figure legend, the reader is referred to the web version of this article.)

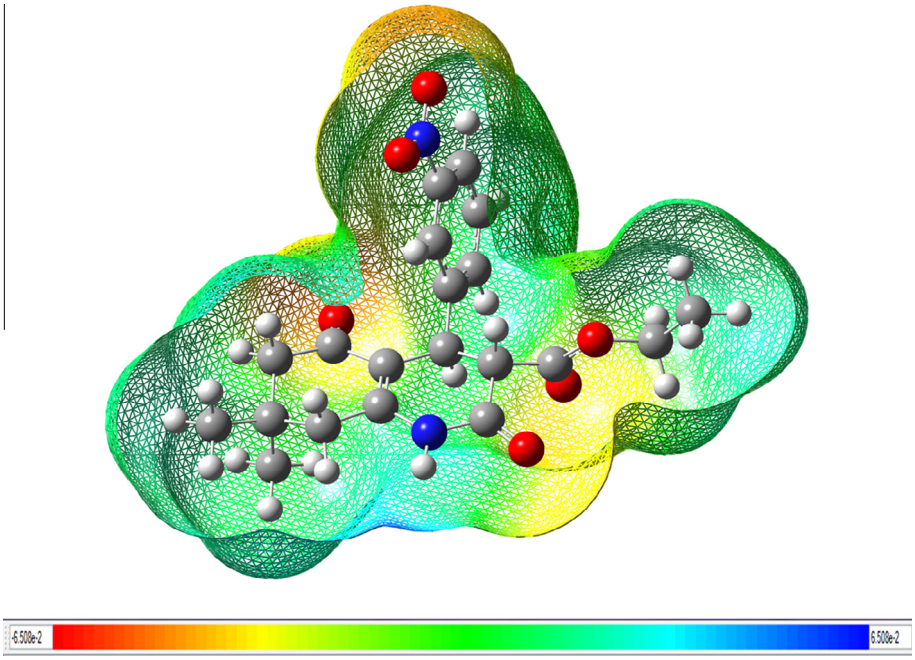

Fig. 4. Molecular electrostatic potential mapped on the isodensity surface in the range from −6.51e−2 (red) to +6.51e−2 (blue) for 2′-NOHQ calculated at the B3LYP/6-311G (d,p) level of theory. (For interpretation of the references to color in this figure legend, the reader is referred to the web version of this article.)

ber of the Raman excitation line and *h*, *c* and *k* are universal constants. The Raman intensities obtained using this relationship match quite nicely with the experimentally observed intensities as shown in Figs. 5 and 6.

Vibrational wavenumbers

Comparison of calculated wavenumbers at the B3LYP/6-311++G (d,p) level with experimental values reveals an overestimation of the wavenumber of the vibrational modes due to neglect of anharmonicity present in real system. Since the vibrational wavenumbers obtained from the DFT calculations are higher than the experimental wavenumbers. Figs. 5–8 show a comparison between experimental and calculated Raman and IR spectra for 2′-NOHQ and 3′-NOHQ.

Ring vibrations

The C—H stretching vibration in ring is usually strong in both the IR and Raman spectra. C—H stretching vibrations of aromatic structures generally occur in the region 3100–2800 cm^{-1} [32] which is the characteristic of C—H stretching vibration. The IR bands observed at 3099, 3090, 3075, and 3065 cm^{-1}, and Raman bands at 3080 and 3069 cm^{-1} are assigned to stretching vibrations of the phenyl ring modes in Ring 3. These bands show a very good agreement with the scaled vibrations obtained. The aromatic in-plane C—H bending and out-of-plane bending vibrations normally occur in the region 1300–1000 cm^{-1} and 750–1000 cm^{-1}, respectively [33]. The υ(CH) wavenumber in Ring 2 is assigned at 2908 and 2769 cm^{-1} in the IR spectra and calculated to be at 2988 and 2935 cm^{-1}.

The $\upsilon(CH_2)$ wavenumber in Ring 1 is assigned at 2857, 2743, 2722, and 2714 cm^{-1} in the IR spectra and at 2775 and 2725 cm^{-1} in the Raman spectra.

The N H stretching vibrations are weaker and sharper, and occur in the region 3500–3300 cm^{-1} [34]. This band is intense in infrared spectra but not observed in Raman spectrum. For 2′-NOHQ, the N H stretch is calculated to be at 3591 cm^{-1} corresponds to 3393 cm^{-1} in IR spectrum. This is a pure mode having 99% contribution from the NH stretching internal coordinate and it is quite overestimated in the calculations. In amides the out-of-plane NH deformation is expected in the region 650 ± 50 cm^{-1} [35] and bands at 685 cm^{-1} in the IR spectra, 660 cm^{-1} in the Raman spectra are assigned as this mode is calculated at 663 cm^{-1}.

The compounds containing nitro group are readily identified by asymmetric bands which observed in the region 1550–1490 cm^{-1}. In the 2′-NOHQ, band found at 1519 cm^{-1} (IR) and 1524 cm^{-1} (Raman) calculated at 1561 cm^{-1} is attributed to NO_2 asymmetric stretching vibrations, and thus coincides well with the experimental observations.

In 2′-NOHQ, the bands at 1290, 1262, 1215, and 1182 cm^{-1} (IR) are assigned to C—H in-plane bending vibrations. Corresponding bands are observed at 1287, 1249, 1211 and 1195 cm^{-1} in 3′-NOHQ. The IR bands at 987, 957, 890, 787 and 743 cm^{-1} are assigned to C—H out-of-plane bending vibrations.

Methyl and methylene group vibrations

Three methyl groups are present in the molecule. Two of them are directly connected to the Ring 1, and the other one is connected to the CH_2 group in the side chain of Ring 2. The asymmetric stretching mode of methyl group is expected to be around 2980 cm^{-1} and symmetric stretching at 2870 cm^{-1} [36,37]. In 2′-NOHQ, the modes appearing at 2997, 2825 and 2790 cm^{-1} are assigned to CH_3 anti-symmetric stretching modes. The CH_3 symmetric stretching normal modes are assigned to bands at 2753, 2736 and 2729 cm^{-1} in the IR spectrum and at 2939, 2926 and 2779 cm^{-1} in the Raman spectrum.

The symmetric and asymmetric bending vibrations of methyl group are normally expected in the regions 1465–1440 cm^{-1}. The asymmetric bending of methyl groups observed at 1427, 1410 and 1386 cm^{-1} in the IR and 1425, 1414 and 1385 cm^{-1} in the Raman spectra are in good agreement with the calculated values. The corresponding experimental wavenumbers for 3′-NOHQ, are observed at 1417 and 1374 cm^{-1} in the IR spectrum.

The asymmetric and symmetric stretching bands of methylene hydrogens ($C42H_2$) in 2′-NOHQ were observed at 2876 and 2781 cm^{-1}.

Table 1
Theoretical and experimental vibrational wavenumbers (cm^{-1}) of 2′-NOHQ.[a]

Calculated			Observed		PED[b]
Unscaled	Scaled 2′-NOHQ	Scaled 3′-NOHQ	IR	Raman	
3591	3468	3468	3393	–	υ(N38—H)(99)
3215	3106	3115	3099	–	R3[υ(C—H)](98)
3197	3088	3096	3090	–	R3[υ(C—H)](100)
3190	3081	3085	3075	3080	R3[υ(C—H](94)
3175	3067	3071	3065	3069	R3[υ(C—H)](98)
3119	3013	3014	3018	3038	Me3[υ(CH_3)](68) + CH_2[υ(C42H)](31)
3105	2999	2999	3001	–	Me3[υ(C43—H45)](94) + CH_2[υ(C42H)](5)
3096	2991	2990	2997	–	Me2[υ(C28—H31)](91)
3093	2988	2989	2908	–	R2[υ(C16—H50)](98)
3093	2987	2986	2876	–	CH_2[υ(C42H)](64) + Me3[υ(C43—H)](33)
3091	2986	2983	2869	–	R1 υ(CH_2)(34) + Me1[υ(C11—H)](39)+ Me2[υ(C28—H)](21)
3087	2982	2982	2857	–	R1[υ(CH_2)](48) + Me1[υ(C11—H)](46)
3086	2981	2975	2825	–	Me2[υ(C28—H)](68) + Me1[υ(C11—H)](21) + R1[υ(C5—H8)](5)
3079	2974	2954	2790	2962	Me1[υ(C11—H)](87) + Me2[υ(C28—H)](12)
3056	2952	2943	2781	2949	CH_2[υ(C42H)](97)
3039	2935	2935	2769	–	υ(C15—H19) (98)
3038	2934	2932	2753	2939	Me3[υ(C43—H)](99)
3036	2933	2931	2743	–	R1[υ(CH_2](96)
3026	2923	2923	2736	2926	Me2[υ(C28—H)](81) + Me1[υ(C11—H13)](5)
3017	2914	2916	2729	2779	Me1[υ(C11—H)](79) + Me2[υ(C28—H)](13)
3010	2908	2905	2722	2775	R1[υ(CH_2)](93)
3002	2899	2899	2714	2725	R1[υ(CH_2)](98)
1787	1774	1780	1719	1720	COO[υ(C18—O40)](66) + R2[υ(C17—O49)](14) + R2 δ(C16)(5)
1767	1754	1760	1618	1614	R2[υ(C17═O49)](62) + COO[υ(C18—O40)](15)
1711	1699	1708	1520	1578	R1[υ(C═O](78) + υ(C2═C3)(6)
1674	1662	1655	–	–	υ(C2═C3)(58) + R1[υ(C═O](7) + R1[$\delta_{as\ ring}$](6)
1645	1633	1645	–	–	R3[υ(C—C)](59) + R3[$\delta_{as\ ring}$](9) + δ(CC21H)(6) + δ(CN35C)(5) + δ(CC23H)(5)
1613	1601	1609	–	–	R3[υ(C—C)](63) + δ(C22H33)(10) + R3[δ_{ring}](9)
1573	1561	1569	–	–	υ(N35O) (79) + ρ(N35C22)(6)
1516	1505	1506	1519	1524	δ($C42H_2$)(68) + Me3[δ(C43H46)]16) + Me3[δ_{as}(HCH)](6)
1513	1502	1501	–	–	R3[υ(C—C)](28) + R3[δ(CC21H)](33) + δ(CN35C)(18)
1512	1501	1500	–	–	Me2[ρ(CH)](51) + Me1[ρ(C6C11)]34) + Me2[δ(C6C28)](5)
1507	1496	1495	–	–	Me2[δ_{as}(CH)](45) + Me1[δ_s(CH)](41)
1498	1487	1488	–	–	Me1[δ_s(CH)](43) + δ($C42H_2$)(31) + Me3[δ_{as}(CH)](18)
1496	1485	1484	–	–	Me1[δ_s(CH)](37) + Me2[δ_{as}(CH)](27) + R1[δ(CH_2)](18)
1493	1482	1478	–	–	R2[δ(CN38)](44) + R2[υ(C2—N38)](23)
1487	1477	1476	–	–	Me1[ρ(C6C11)](50) + Me2[ρ(CH)](35)
1486	1475	1476	–	–	Me3[δ_{as}(C43H)](91) + δ(C42C43)(7)
1474	1463	1462	1468	1466	δ(C22H33)(22) + δ(CC23H)(20) + R3[υ(C—C)](29) + R2[δ(C15H)](6) + δ(CN35C)(5)
1473	1462	1462	–	–	R1[δ(CH_2)](72) + Me2[δ_{as}(CH)](12) + Me1[δ_s(CH)](7)
1464	1453	1453	1449	1477	R1[δ(CH_2)](94)
1427	1417	1418	1427	1425	Me2[δ_s(C28)](50) + Me1[δ_s(C11)](37)
1426	1416	1415	1410	1414	Me3[δ_s(CH)](50) + ω($C42H_2$)(26) + υ(C42C)(13)
1405	1395	1394	–	–	Me1[δ(C11)](54) + δ(C28HC)(38)
1399	1389	1391	1386	1385	ω($C42H_2$)(43) + Me3[δ_s(CH_3)](37)
1391	1381	1376	–	–	R2[δ(C15H)](36) + R2[ρ(C15H)](12) + δ(CN35C)(6)
1387	1377	1363	–	–	R1[ω(CCH)](42) + R1[υ(C—C)](15) + R1[$\delta_{as\ ring}$](6)
1378	1368	1358	1355	1358	υ(N35O)(55) + δ(NO_2)(15) + R3[υ(C22—N35)](15)
1363	1353	1352	1354	1344	R2[ω(C15H)](22) + R2[γ(C15H)](13) + R2[δ(C16H)](9) + R2[ω(C16H)](9) + R2[γ(C16H)](7) + υ(C16—C18)](5) + ω($C42H_2$)(5) + R2[ρ(C16)](5) + R2[υ(C15—C16](5)
1346	1336	1335	–	–	R1[υ(C—C)](30) + R1[δ(C═O)](7) + R2[υ(C3—C15)](7) + R2[υ(C17—N38)](5) + R2[δ(C16H)](5) + R2[δ_{ring}](5)
1338	1328	1330	–	–	R3[υ(C—C)](66) + δ(CC21H)(14) + δ(C22H33)(6)
1325	1316	1313	–	–	R2[ω(C16H)](20) + R2[γ(C16H)](14) + R2[δ(C16H)](10) + R1[γ(CC1H)](6)

1323	1314	1306	–	–	R1[ω(CH_2)](39) + R2[ω(C16H)](8) + R1[γ(CH_2)](7) + R2[γ(C16H)](5)
1311	1301	1297	–	–	R1[ω(CH_2)](34) + R1[γ(CH_2)](21) + υ(C6—C28)(6) + R1[υ(C4—C5)](5)
1301	1292	1291	1290	1294	R2[υ(C17—N38)](19) + COO[υ(C18—O41)](12) + R2[ω(C15H)](6) + R2[υ(C16—C17](6) + R2[δ(CO)](5)
1298	1288	1290	–	–	γ($C42H_2$)(83) + Me3[δ(C42C43)](7)
1281	1271	1269	–	–	R1[υ(C—C)](28) + R1[γ(CH_2)](24) + R1[ω(CC6C)](12) + Me2[δ(C6C28)](7) + Me1[δ_{as}(CH)](7)
1271	1262	1263	1262	1261	R3[υ(C—C)](20) + R2[δ(C15H)](13) + δ(CC21H)(11) + δ(CN35C)(10) + R2[υ(C17—N38)](9) + R2[ρ(C15H)](7)
1248	1239	1230	1235	1238	R2[υ(C2—N38)](16) + R2[ω(C15H)](10) + R2[δ(CH39N38)](8) + R2[ω(C16H)](8) + R2[δ(C15H)](6) + R1[δ_{ring}](6)
1238	1229	1220	1216		R2[υ(C17—N38)](10) + R2[ω(C15H)](8) + R2[ω(C16H)](6) + R2[δ(CO)](6) + R2[δ(C15H)](6) + R1[δ_{ring}](5) + R1[υ(C3—C4)](5)
1212	1203	1212	1215	1217	υ(C15—C20)(32) + R3[υ(C22—C25)](19) + R3[δ_{ring}](7) + δ(CN35C)(6) + δ(CC23H)(6) + R2[δ_{ring}](5)
1192	1183	1183	1182	1190	R3[δ(CCH)](48) + δ(CN35C)(9) + COO[υ(C18—O41)](7) + R3[υ(C21—C23)](6) + R2[δ(C16H)](5)
1188	1180	1176	–	–	COO[υ(C18—O41)](20) + R2[δ(C16)](15) + δ(C22H33)(10) + R2[γ(C16H)](6) + δ(CC23H)(6)
1181	1173	1171	1170	1188	R2[υ(C2—N38)](9) + R1[γ(CC1H)](9) + υ(C6—C11)(8) + Me2[ρ(C6C28)](15) + R1[ω(CC1H)](6) + δ(C6C11)(5) + R1[δ(CC6C)](5)
1176	1168	1168	–	–	R1[γ(CH_2)](36) + Me2[ρ(C6C28)](5)
1176	1167	1164	–	–	ρ($C42H_2$)(48) + Me3[δ(C42C43)](25) + Me3[ρ(C42C43)](9) + γ($C42H_2$)(5) + Me3[δ_{as}(CH)](5)
1164	1156	1138	–	1150	R3[υ(C—C)](26) + δ(C22H33)(15) + R3[υ(C22—N35)](8) + δ(CC23H)(6) + δ(CC20C)(5)
1149	1140	1128	1141	1134	R1[γ(CC5H)](17) + υ(C6—C28)(12) + R1[ρ(CC6C)](10) + υ(C6—C11)(8) + R1(δ_{ring})(6) + R1[ρ(CC5H)](6) + R1[γ(CC1H)](5) + δ(C6C11)(5)
1136	1128	1117	–	–	Me3[ρ(C42C43)](37) + υ(C42C)(20) + δ($C42H_2$)(13) + δ(CO41C)(6) + υ(C42C)(5)
1133	1125	1104	–	–	R1[υ(C1—C2)](20) + R2[υ(C—C)](25) + R2[δ_{ring}](9)
1105	1097	1095	1100	1099	R2[υ(C15—C16](27) + R3[δ_{ring}](10) + R1[υ(C4—C5)](6) + R3[υ(C22—N35)](6)
1090	1082	1084	–	1078	R3[δ_{ring}](38) + R3[υ(C22—N35)](12) + R2[υ(C15—C16](10)
1070	1062	1047	1066	1069	R3[υ(C—C)](61) + δ(CN35C)(5)
1054	1047	1027	–	1047	υ(C42C)(18) + R1[υ(C4—C5)](11) + R2[υ(C15—C16](8) + R1[δ_{ring}](13)
1034	1027	1025	–	–	υ(C42C)(30) + R2[υ(C15—C16](7) + Me2[δ(C6C28)](6) + Me1[δ_{as}(CH)]5) + δ(C6C11)(5) + Me3[ρ(C42C43)](5)
1033	1025	1010	1015	1018	Me2[δ(C6C28)](34) + Me1[δ_{as}(CH)](20) + υ(C42C)(13)
1008	1001	997	–	–	O(H34—C21—C26—C23)(38) + O(H33—C23—C25—C26)(24) + O(H24—C20—C23—C21)(15) + R3[$puck_{ring}$](14) + O(H27—C22—C25—C22)(5)
1000	992	995	987	988	υ(C16—C18)](16) + υ(C42C) (13) + R1[υ(C—C)](10) + R2[δ_{ring}](5) + R1[υ(C1—C6)](5) + R2[υ(C17—N38)](5)
983	976	974	–	978	R1[ρ(CCH)](15) + δ(C6C11)(12) + υ(C6—C11)(10) + υ(C16—C18)](8) + R2[υ(C3—C15)](5) + υ(C42C)(5) + R1[υ(C4—C5)](5)
977	970	948	–	–	O(H27—C22—C25—C22)(34) + O(H24—C20—C23—C21)(23) + O(H33—C23—C25—C26)(19) + O(H34—C21—C26—C23)(6) + R3[τ_{ring}](5)
951	944	945	957	941	Me2[ρ(C6C28)](40) + υ(C6—C)(24) + Me1[δ_{as}(CH)]12) + δ(C6C11)(10)
944	937	941	–	–	R1[υ(C—C](31) + Me2[ρ(C6C28)](16) + δ(C6C11)(17) + Me1[δ_{as}(CH)]7) + R1[ρ(CC5H)](5)
941	934	937	932	–	R2[O(O49—C16—N38—C17)](11) + R2[ρ(C16)](11) + R3[δ_{ring}](8) + R2[υ(C16—C17](6) + δ_{oop}(C18—C16)(5) + R2[ρ(C15H)](5)
928	921	927	–	–	R1[υ(C—C)](31) + υ(C6—C28)(15) + R1[ρ(CCH)](19) + Me1[δ_{as}(CH)](5)
903	897	921	–	–	R1[ρ(CCH)](50) + O(C4—O9—C3—C5)(10) + δ_{oop}(C2=C3)(5)
893	886	907	890	891	O(H24—C20—C23—C21)(23) + O(H27—C22—C25—C22)(20) + R3[$puck_{ring}$](10) + O(N35—C20—C25—C22)(7) + O(H34—C21—C26—C23)(5)
883	877	896	–	–	δ(NO_2)(27) + R3[δ_{ring}](21) + R3[υ(C22—N35)](8) + υ(C15—C20)(6)
876	869	869	861	864	υ(C42C)(37) + Me3[ρ(C42C43)](12) + O(H24—C20—C23—C21)(5) + O(H27—C22—C25—C22)(5) + ω($C42H_2$)5)
845	839	840	839	845	R1[δ_{ring}](11) + δ_{oop}(C2=C3)(8) + R2[$puck_{ring}$](8) + δ(C18O41)(5) + δ(CO41C)(5)
839	833	832	–	–	δ(NO_2)(26) + υ(C15—C20)(13) + R3[υ(C—C)](12)+R2[ρ(C15H)](4)
824	818	817	–	–	υ(C6—C28)(23) + R1[δ_{ring}](9) + δ(C18O41)(5) + δ_{oop}(C2=C3)(5)
812	806	808	813	814	ρ($C42H_2$)(43) + Me3[δ(C42C43)](38) + γ($C42H_2$)(14)
803	797	808	787	793	O(N35—C20—C25—C22)(26) + δ_{oop}(NO_2)(20) + O(H34—C21—C26—C23)(16) + R3[$puck_{ring}$](14) + O(H24—C20—C23—C21)(6) + O(H33—C23—C25—C26)(6)
772	766	764	–	754	R3[$puck_{ring}$](9) + O(H33—C23—C25—C26)(8) + δ_{oop}(C15C20) (6) + R2[υ(C16—C17](6) + υ(C6C28)(6) + δ(C18O41)(5)
758	752	735	743	747	R3[$puck_{ring}$](25) + O(H33—C23—C25—C26)(16) + O(N35—C20—C25—C22)(10) + δ_{oop}(C18—C16)(9) + O(H27—C22—C25—C22)(6)
727	721	721	–	720	R3[$puck_{ring}$](17) + δ_{oop}(NO_2)(14) + R2[δ_{ring}](9) + R2 O(O49—C16—N38—C17)(6) + R1[υ(C3—C4)](6) + O(H34—C21—C26—C23)(5)
722	716	713	–	–	R3[$puck_{ring}$](29) + δ_{oop}(NO_2)(10) + δ_{oop}(C15C20)(5)
716	710	691	–	–	δ_{oop}(C18—C16)(22) + R2[O(O49—C16—N38—C17)](13) + R3[$puck_{ring}$](7) + R3[$\delta_{as\ ring}$](5)
680	675	689	699	694	R3[δ_{ring}](36) + δ(NO_2)(9) + R3[$puck_{ring}$(7) + R3[υ(C22—N35)](6) + R3[υ(C20—C22)](5)
668	663	658	685	660	R2[O(H39—C2—C17—N38)(29) + R2 O(O49—C16—N38—C17)(16) + R3($puck_{ring}$)(7) + R2[τ_{ring}](5)
654	649	644	657	644	O(C4—O9—C3—C5)(18) + R3($\delta_{as\ ring}$)(14) + R3(δ_{ring})(13) + R1[ρ(CH_2)](5)
627	623	621	–	–	δ_{oop}(C2=C3)(21) + R2[$puck_{ring}$](11) + R3[($\delta_{as\ ring}$)](9) + O(C4—O9—C3—C5)(8) + R2[O(H39—C2—C17—N38)](5) + R1[δ(C=O)](5)
619	614	613	609	–	R2[O(H39—C2—C17—N38)](14) + R3($puck_{ring}$)(8) + R2[δ(C=O)](7) + O(C4—O9—C3—C5)(6) + R1[δ(C=O)](6) + R3[($\delta_{as\ ring}$)](5) + δ_{oop}(C18O41)(5)
603	599	591	602	598	δ_{oop}(C2=C3)(21) + R3[$puck_{ring}$](6) + R2 O(H39—C2—C17—N38)(6) + δ(CC20C)(6) + R2[$puck_{ring}$](6) + R2 O(O49—C16—N38—C17)(5) + R3[$\delta_{as\ ring}$](5) + R2[ρ(C15H19)](5)
575	571	569	577	–	R2[O(H39—C2—C17—N38)](20) + δ_{oop}(C2=C3)(16) + R2[δ_{ring}](10)
562	557	559	566	569	ρ(N35C22)(17) + O(N35—C20—C25—C22)(10) + δ_{oop}(C2=C3) (10) + R3[τ_{ring}](15) + R3[$puck_{ring}$](7)
556	552	527	545	548	R3[τ_{ring}](14) + R3[$puck_{ring}$](8) + R1[δ(C=O)](10) + R1[$\delta_{as\ ring}$](6) + δ_{oop}(C15C20)(9)
512	509	507	517	519	R1[$\delta_{as\ ring}$](18) + δ(C18OO)(10) + δ(CC20C)(7) + R2[O(O49—C16—N38—C17)](6)
508	505	499	–	–	R2[δ_{ring}](15) + R1[δ(C=O)](10) + R1(δ_{ring})7) + R1[δ(CC6C)](7) + R3[τ_{ring}](6)
490	487	488	485	484	R2[δ(CO)](15) + R3[τ_{ring}](13) + δ_{oop}(C2=C3) (9) + δ_{oop}(C15C20)(7) + R1[$\delta_{as\ ring}$](12) + R2[O(H39—C2—C17—N38)](6)
467	464	463	464	459	R3[τ_{ring}](13) + R1[δ(CC6C)](16) + R1[$\delta_{as\ ring}$(13) + δ(C18O41) (6) + R1($\delta_{as\ ring}$)(5) + δ(C18OO) (5) + δ_{oop}(C2=C3)(5)

(*continued on next page*)

Table 1 (*continued*)

Calculated			Observed		PED[b]
Unscaled	Scaled 2′-NOHQ	Scaled 3′-NOHQ	IR	Raman	
431	428	429	424	423	R1[ω(CC6C)](26) + R1[$\delta_{as\ ring}$](17) + R1[ρ(CC6C)](5) + R2[δ(CO)](5)
415	412	425	–	–	R3[τ_{ring}](53) + O(N35—C20—C25—C22)(21) + ρ(N35C22)(5)
402	399	393	–	–	R3[υ(C22—N35)](18) + R1[ρ(CC6C)](17) + R3[δ_{ring}](8) + R3[τ_{ring}](7)
393	390	392	–	–	R1[δ(CC6C)](13) + δ(C42H_2)(9) + R2[δ_{ring}](8) + R1[$\delta_{as\ ring}$](8) + R1[ρ(CC6C)](7) + R1[ω(CC6C)](5) + R3[υ(C22—N35)](5)
383	380	378	–	–	δ(C42H_2)(33) + R1[ρ(CC6C)](20) + δ(C18O41)(5)
355	352	353	–	–	R3[τ_{ring}](10) + R1[ρ(CC6C)](8) + R1[ω(CC6C)](7) + R1[δ(C=O)](7) + R2[δ_{ring}](6) + δ(C42H_2)(5) + R2[δ_{ring}](5)
344	342	345	–	–	R1[δ(CC6C)](30) + R1[$\delta_{as\ ring}$](11) + R1[ω(CC6C)](8)
318	315	313	–	–	δ(CC20C)(17) + δ_{oop}(C2=C3)(10) + R2[τ_{ring}](9) + δ(N35C)(9) + R1[δ(CC6C)](6) + ρ(N35C22)(5)
299	297	305	–	–	δ(CC20C)(13) + δ(N35C)(12) + δ(CO41C)(10) + δ(C18OO)(9) + R2 ρ(C16)(6) + R1[υ(CC6C)](6) + R1[δ(CC6C)](5)
287	284	284	–	–	R1[υ(CC6C)](21) + Me2[τ(CH_3)](8) + δ(CO41C)(6) + Me1[τ(CH_3)](5) + R1[δ(C=O)](5)
276	274	276	–	–	Me3[τ(CH_3)](37) + τ(C18O41)(12) + R3[υ(CH)](7) + R2[δ(CO)](5) + Me2[τ(CH_3)](5)
270	268	272	–	–	Me3[τ(CH_3)](17) + Me1[τ(CH_3)](15) + Me2[τ(CH_3)](8) + R3[τ_{ring}](6) + δ(CO41C)(5)
252	250	253	–	–	Me1[τ(CH_3)](25) + R3[τ_{ring}](13) + R1[υ(CC6C)](10) + O(N35—C20—C25—C22) (9) + ρ(N35C22)(5)
247	245	247	–	–	Me3[τ(CH_3)](18) + R2[δ_{ring}](7) + O(N35—C20—C25—C22)(6) + δ(N35C)(6) + υ(C15—C20)(5) + R3[$\delta_{as\ ring}$](5) + R2[τ_{ring}](5) + R3[τ_{ring}](5)
227	226	227	–	–	Me1[τ(CH_3)](35) + Me2[τ(CH_3)](25)
220	218	219	–	–	Me2[τ(CH_3)](16) + R1[$\delta_{as\ ring}$](7) + Me3[τ(CH_3)](7) + O(N35—C20—C25—C22)(6)
215	213	208	–	–	Me2[τ(CH_3)](25) + R1[υ(CC6C)](15) + O(N35—C20—C25—C22)(10) + Me3[τ(CH_3)](5)
204	202	201	–	–	δ(N35C)(21) + R2[ρ(C16)](9) + υ(C16—C18)](7) + R2[δ_{ring}](7) + δ(CC20C)((7) + O(N35—C20—C25—C22)(5)
168	167	169	–	–	R2[O(H39—C2—C17—N38)](24) + R2[τ_{ring}](18) + R1[δ_{ring}](15) + R2[$puck_{ring}$](15) + R3[δ_{ring}](5)
162	161	165	–	–	R2[O(H39—C2—C17—N38](19) + R2[τ_{ring}](15) + τ(C18O41) (12) + R2[$puck_{ring}$](9) + R1[δ_{ring}](5) + R1[τ_{ring}](5)
152	151	163	–	–	δ(CO41C)(13) + τ(C18O41)(10) + δ(C18O41)(7) + O(N35—C20—C25—C22)(7) + R2[$puck_{ring}$](7)+ δ(C42H_2) (6) + R3[τ_{ring}](5)
130	129	133	–	–	R3[τ_{ring}(C21)](32) + O(N35—C20—C25—C22)(13) + R3[τ_{ring}](21)
116	115	110	–	–	R1[τ_{ring}](41) + R2[O(H39—C2—C17—N38)](8) + R1[δ_{ring}](12) + R2[τ_{ring}](7) + δ_{oop}(C2=C3)(5) + R2[$puck_{ring}$)(5)
102	101	94	–	–	R1[τ_{ring}](23) + τ(C18C16)(11) + R1[δ_{ring}](10) + τ(C18O41)(7) + R2[γ(C16H)](7) + R2[O(H39—C2—C17—N38)](5)
90	90	83	–	–	R1[τ_{ring}](30)+ τ(C18C16)(14) + NO_2[τ(NC)](7) + R3[τ_{ring}](6) + R2[γ(C16H)](6) + R1[δ_{ring}](5)
80	79	74	–	–	NO_2[τ(NC)](18) + R3[τ_{ring}](11) + R2[τ_{ring}](9) + R2 O(H39—C2—C17—N38)(9) + R2[$puck_{ring}$](6)
64	63	63	–	–	NO_2[τ(NC)](20) + τ(C18O41)(10) + R2[$puck_{ring}$](8) + τ(O41C42)(7) + δ_{oop}(C2=C3)(6) + τ(C18C16)(6)
61	61	55	–	–	R1[τ_{ring}](16) + R[$puck_{ring}$](15) + R2 O(H39—C2—C17—N38)(15) + R2[τ_{ring})(13) + τ(O41C42)(8) + [τ(NO_2)](5) + R3[τ_{ring}](5)
52	52	40	–	–	R2[τ_{ring}](18) + δ_{oop}(C15C20)(14) + R1[τ_{ring}](20) + R2[O(H39—C2—C17—N38)](6) + R2[γ(C15H)](6)
47	46	33	–	–	R2[τ_{ring}](32) + R2[τ_{ring})(17) + NO_2[τ(NC)(13) + R1[τ_{ring}](6) + R2[O(H39—C2—C17—N38)](6)
30	30	27	–	–	NO_2[τ(NC)](38) + R3[τ_{ring}](14) + R2[τ_{ring}](13) + δCC20C)(7) + R2[ρ(C15H)](6)
17	17	21	–	–	R2[τ_{ring}](51) + R2[$puck_{ring}$](20) + NO_2[τ(NC)](9) + δ(CC20C)(5)
13	12	17	–	–	τ(C18C16)(32) + τ(O41C42)(30) + R2[τ_{ring}](10) + NO_2[τ(NC)](5)

[a] Proposed assignment and potential energy distribution (PED) for vibrational normal modes. Types of vibration: υ, stretching; δ, deformation; O, out-of-plane bending; ω, wagging; γ, twisting; ρ, rocking; τ, torsion.
[b] Potential energy distribution (contributing ⩾5) for 2′-NOHQ.

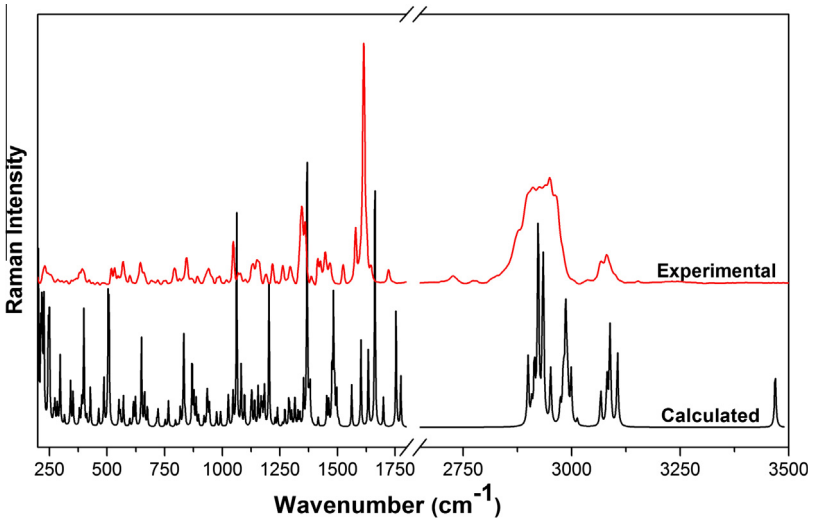

Fig. 5. FT-Raman spectrum of 2′-NOHQ.

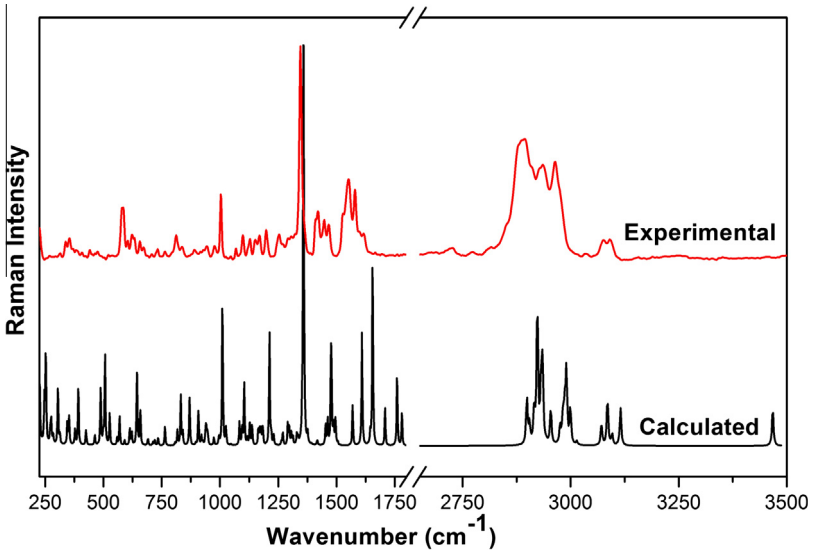

Fig. 6. FT-Raman spectrum of 3′-NOHQ.

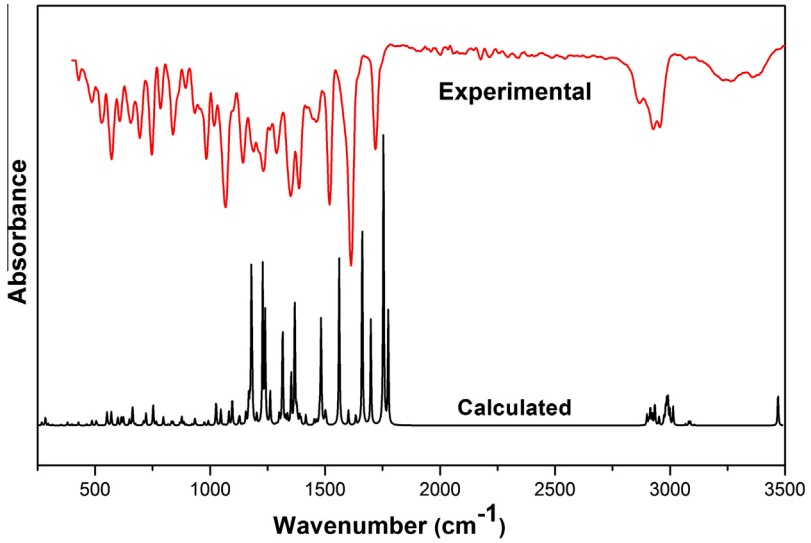

Fig. 7. FT-IR spectrum of 2′-NOHQ.

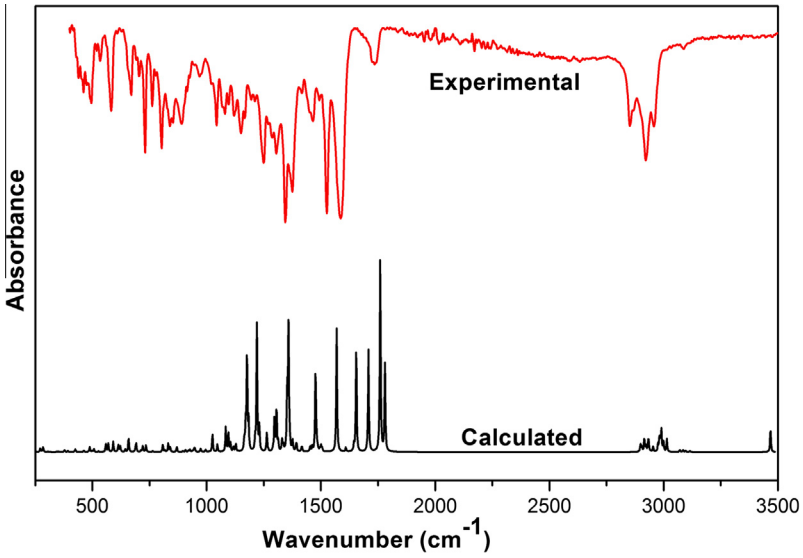

Fig. 8. FT-IR spectrum of 3′-NOHQ.

Carbonyl group vibrations

Esters show a very strong band for the C═O group in the range of 17,501,735 cm^{-1}. Stretching mode of C18O40 in 2′-NOHQ, is observed at 1719 cm^{-1} in IR as a very strong band and at 1720 cm^{-1} in Raman as a weak band. A very strong band of the amide carbonyl stretching vibration is observed at 1618 cm^{-1} in the IR and 1614 cm^{-1} in the Raman spectra. The cyclic ketone appears at 1520 cm^{-1} in the IR spectra and 1578 cm^{-1} in the Raman spectra. In 3′-NOHQ, these modes appear at 1736, 1587, 1525 cm^{-1} in the IR and 1612, 1578, 1551 cm^{-1} in the Raman spectra. It is observed from Table 1 that the calculated vibrational frequencies of both the isomers are very close to the experimental values.

NMR spectra

^{1}H and ^{13}C NMR chemical shifts were calculated at the B3LYP/6-311++G (d,p) level. The experimental and theoretical values of ^{1}H and ^{13}C NMR spectra of 2′-NOHQ are given in Table 2. The ^{13}C and ^{1}H NMR spectra in DMSO-*d6* are presented in Fig. 9. The singlet observed at 10.86 ppm is assigned to N H and this has been computed to be at 6.12 ppm. The phenyl protons resonate as the multiplet at 7.49–8.26 ppm experimentally and these have been predicted in the range 7.33–9.50 ppm. A singlet at 2.35 and 2.40 ppm correspond to the methylene hydrogens of the ring and the singlet at 4.09 to the methylene protons of the side chain. In the ^{13}C NMR spectrum, C18 in Ring 2 and C22 in Ring 3 appear at lower chemical shift of 161.8 and 133.3 ppm due to neighboring electronegative oxygen and nitrogen atoms. C42 appears at higher field of 54.8 ppm due the methyl and the ester groups attached to it. The carbonyl carbon C4 at 191.30 ppm, methyl carbons C11, C28, and C43 at 26.1, 27.6, and 16.2 are in good agreement with the predicted chemical shifts. It is observed from Table 2 that the predicted chemical shift values are in closer agreement with the experimental values. The experimental and theoretical values of ^{1}H and ^{13}C NMR for 3′-NOHQ are given in the Table S2 as a supplementary material.

Table 2
Observed and calculated NMR chemical shifts (δ ppm) for 2′-NOHQ.

Atom	δ (Calculated)	δ (Expt.)	Δ[a]	Atom	δ (Calculated)	δ (Expt.)	Δ[a]
C1	46.36	46.8	−0.44	H7	2.49	2.35	0.14
C2	153.64	115.2	38.44	H8	1.70	2.4	−0.70
C3	118.92	148.8	−29.88	H10	1.89	2.4	−0.51
C4	203.83	191.6	12.23	H12	0.75	1.11	−0.36
C5	55.89	32.3	23.59	H13	0.77	1.11	−0.34
C6	43.23	30.1	13.13	H14	1.35	2.35	−1.00
C11	31.59	26.1	5.49	H19	4.93	4.45	0.48
C15	59.07	31.9	27.17	H24	8.38	7.24	1.14
C16	56.06	47.4	8.66	H27	9.50	7.47	2.03
C17	171.51	178.1	−6.59	H29	0.45	1.11	−0.66
C18	186.62	161.8	24.82	H30	0.55	1.11	−0.56
C20	140.98	135.3	5.68	H31	1.22	1.11	0.11
C21	146.61	122.7	23.91	H32	0.69	1.11	−0.42
C22	161.08	133.3	27.78	H33	7.33	7.08	0.25
C23	140.39	129.5	10.89	H34	7.53	7.44	0.09
C25	140.02	115.2	24.82	H39	6.12	10.86	−4.74
C26	131.96	121.5	10.46	H44	2.61	1.23	1.38
C28	25.63	27.6	−1.97	H45	2.22	1.23	0.99
C42	37.46	54.8	−17.34	H46	1.87	1.23	0.64
C43	24.83	16.2	8.63	H47	9.56	4.09	5.47
				H48	8.30	4.09	4.21
				H50	3.76	6.05	−2.29

[a] $\delta_{calculated} - \delta_{expt}$.

Thermodynamic properties

Thermal properties such as thermal diffusivities, specific heat capacities etc. of octahydroquinolindiones are crucially important from the viewpoint not only of fundamental aspects for academia but also of various processing and applications of the octahydroquinolindiones. On the basis of vibrational analysis and statistical thermodynamics, the standard thermodynamic functions: heat capacity ($C°_{p,m}$), entropy ($S°_{m}$) and enthalpy ($H°_{m}$) were obtained and listed in Table 3. As observed from Table 3, values of heat capacity, entropy and enthalpy increase with the increase of temperature from 100 to 500 K which is attributed to the enhancement of molecular vibration with increase in the temperature.

The correlation between these thermodynamic properties and temperatures T are shown in Fig. 10. The correlation equations for octahydroquinolindiones are as follows:

$$C°_{p,m} = Y = 1.4506 + 0.30045T - 4.56^{*}10^{-5}T^{2} \quad (R^{2} = 0.99953)$$

$$S°_{m} = Y = 60.6378 + 0.32287T - 3.88357^{*}10^{-5}T^{2} \quad (R^{2} = 0.99999)$$

$$H°_{m} = Y = 249.5756 + 0.00344T + 1.3922910^{-4}T^{2} \quad (R^{2} = 0.99999)$$

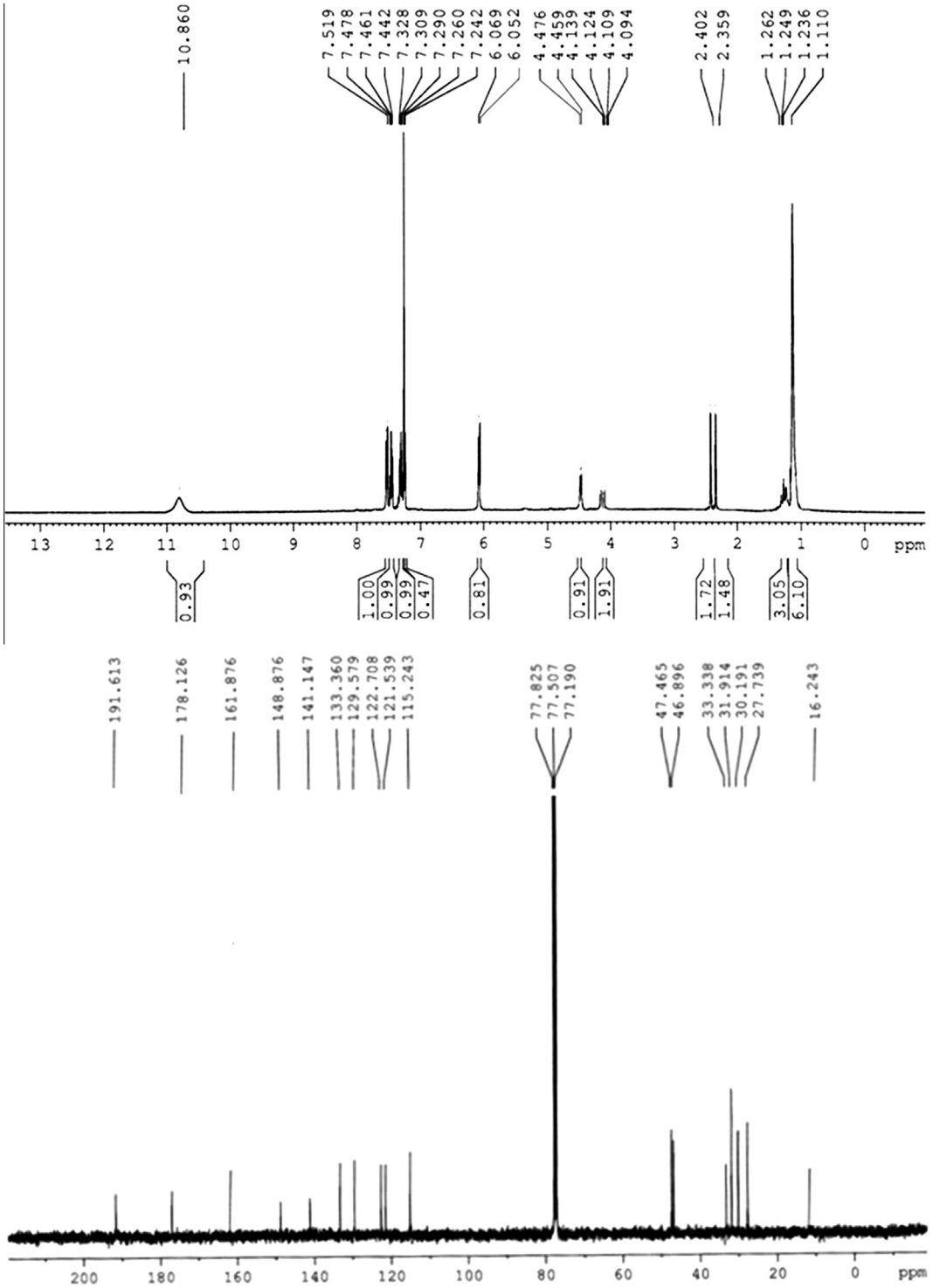

Fig. 9. ^{1}H NMR and ^{13}C NMR spectra of 2′-NOHQ.

Table 3
Thermodynamic properties of 2′-NOHQ at different temperatures at B3LYP/6-311++G (d,p) level.

T (K)	H_m (kcal/mol)	$C_{p,m}$ (Cal/mol K)	S_m (Cal/mol K)
100	251.324	31.627	92.439
200	255.818	58.547	123.897
300	263.108	87.469	153.867
400	273.282	115.523	183.512
500	286.08	139.685	212.414

These equations could be used for the further studies on the title compound. For instance, when the interaction of octahydroquinolindiones with any other compound is studied, these thermodynamic properties could be obtained from the above equations and then can be used to calculate the change in Gibbs free energy of the reaction, which will in turn help to judge the spontaneity of the reaction.

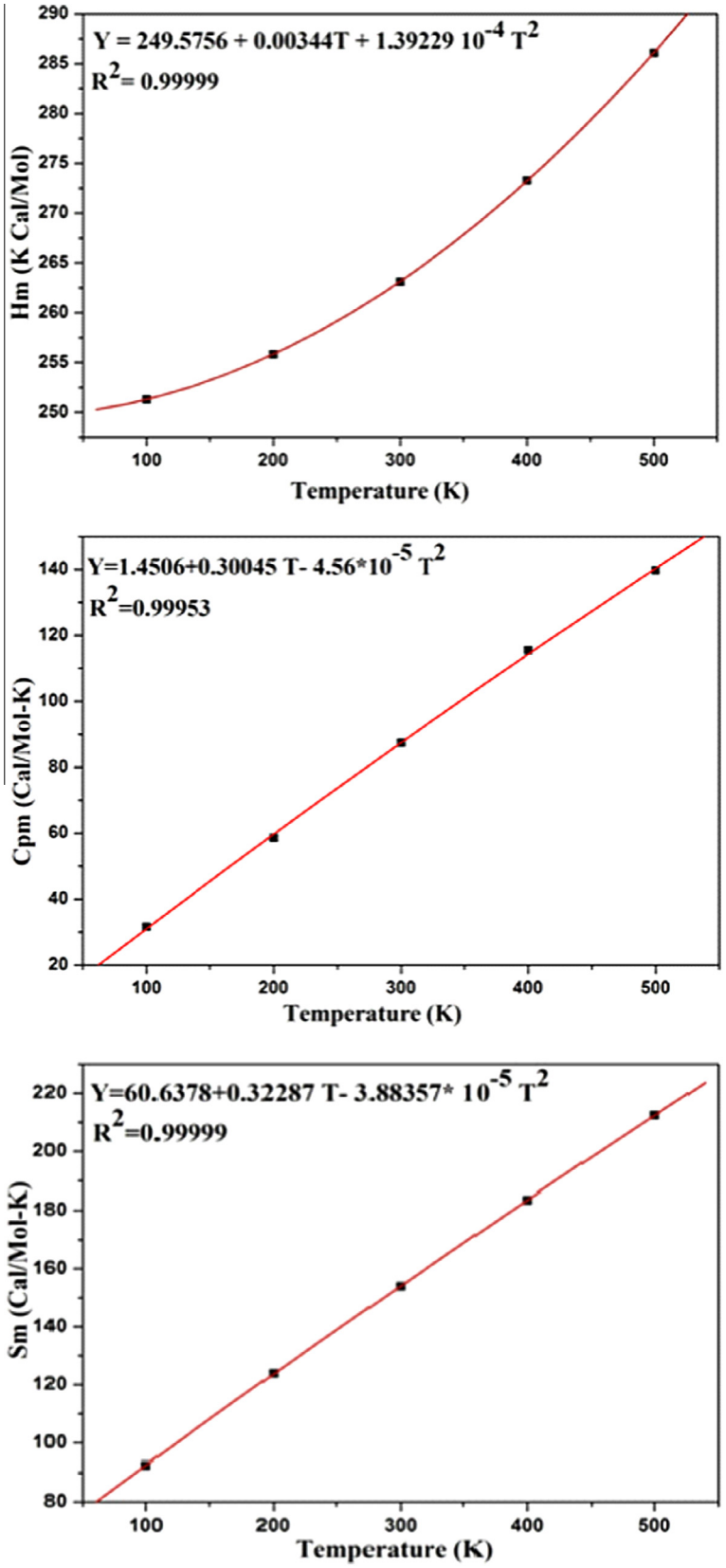

Fig. 10. Temperature dependence of the thermodynamic values $H°_m$, $C°_{p,m}$, and $S°_m$ of 2′-NOHQ.

Conclusions

Vibrational, electronic, NMR, reactivity and structural aspects of 2′-NOHQ and its isomer 3′-NOHQ were studied in detail based on B3LYP/6-311++G (d,p) method, and the results were compared with the experimental results. A detailed normal coordinate analysis of all the normal modes along with PED assignment has been made indicating the composition of each normal mode. Comparison between the calculated and experimental vibrational frequencies indicate that the results are in good agreement with experimental values. The ^{13}C and ^{1}H NMR spectra of the compounds were recorded, assignment of the chemical shifts were done for calculated and experimental values. The thermodynamic properties of the title compounds at different temperatures were calculated, and the correlations between $C°_{p,m}$, $S°_{m}$, $H°_{m}$ and temperatures have also been given for both the compounds.

Appendix A. Supplementary material

Supplementary data associated with this article can be found, in the online version, at http://dx.doi.org/10.1016/j.saa.2014.09.021.

References

[1] (a) G. Claassen, E. Brin, C. Crogan-Grundy, M.T. Vaillancourt, H.Z. Zhang, S.X. Cai, J. Drewe, B. Tseng, S. Kasibhatla, Cancer Lett. 274 (2009) 243–249;
(b) Z.-J. Ni, P. Barsanti, N. Brammeier, A. Diebes, D.J. Poon, S. Ng, S. Pecchi, K. Pfister, P.A. Renhowe, S. Ramurthy, A.S. Wagman, D.E. Bussiere, V. Le, Y. Zhou, J.M. Jansen, S. Ma, T.G. Gesner, Bioorg. Med. Chem. Lett. 16 (2006) 3121–3124.
[2] A. Afonso, J. Weinstein, M.J. Gentles, (Schering Corp.) WO 9203327, 1992.
[3] (a) R.M. Forbis, K.L. Rinehart Jr., J. Am. Chem. Soc. 95 (1973) 5003–5013;
(b) H.M. Hassanin, S.M. El-edfawy, Heterocycles 85 (2012) 2421–2436.
[4] J.C. Lanter, Z. Sui, M.J. Macielag, J.J. Fiordeliso, W. Jiang, Y. Qiu, S. Bhattacharjee, P. Kraft, T.M. John, D. Haynes-Johnson, E. Craig, J. Clancy, J. Med. Chem. 47 (2004) 656–662.
[5] G. Anquetin, J. Greiner, P. Vierling, Tetrahedron 61 (2005) 8394–8404.
[6] P.D. Duarte, R.P. Severino, P.C. Vieira, D. Brömme, A.G. Corrêa, 4th Brazilian Symposium on Medicinal Chemistry, Brazilian Chemical Society (SBQ).
[7] C.T. Alabaster, A.S. Bell, S.F. Campbell, P. Ellis, C.G. Henderson, D.A. Roberts, K.S. Ruddock, G.M. Samuels, M.H. Stefaniak, J. Med. Chem. 31 (1988) 2048–2056.
[8] Farhanullah, S.Y. Kim, E.-J. Yoon, E.-C. Choi, S. Kim, T. Kang, F. Samrin, S. Puri, J. Lee, Bioorg. Med. Chem. 14 (2006) 7154–7159.
[9] US 8247420 B2, US 12/124, 985, 2012.
[10] F. Domínguez-Fernandez, J. Lopez-Sanz, E. Perez-Mayoral, D. Bek, R.M. Martın-Aranda, A.J. Lopez-Peinado, J. Cejka, Chem. Cat. Chem. 1 (2009) 241–243.
[11] M. Marull, O. Lefebvre, M. Schlosser, Eur. J. Org. Chem. (2004) 54–63. and references cited therein.
[12] K.Y. Lee, J.N. Kim, Bull. Korean Chem. Soc. 23 (2002) 939–940.
[13] J. Ferguson, F. Zeng, N. Alwis, H. Alper, Org. Lett. 15 (2013) 1998–2001.
[14] S.H.S. Azzam, A. Siddekha, M.A. Pasha, Tetrahedron Lett. 53 (2012) 6306–6309.
[15] P. Hohenberg, W. Kohn, Phys. Rev. 136B (1964) 864–871.
[16] M.J. Frisch, G.W. Trucks, H.B. Schlegel, G.E. Scuseria, M.A. Robb, J.R. Cheeseman, J.A. Montgomery, T. Vreven, K.N. Kudin, J.C. Burant, J.M. Millam, S.S. Iyengar, J. Tomasi, V. Barone, B. Mennucci, M. Cossi, G. Scalmani, N. Rega, G.A. Petersson, H. Nakatsuji, M. Hada, M. Ehara, K. Toyota, R. Fukuda, J. Hasegawa, M. Ishida, Nakajima, Y. Honda, O. Kitao, H. Nakai, M. Klene, X. Li, J.E. Knox, H.P. Hratchian, J.B. Cross, C. Adamo, J. Jaramillo, R. Gomperts, R.E. Stratmann, O. Yazyev, A.J. Austin, R. Cammi, C. Pomelli, J.W. Ochterski, P.Y. Ayala, K. Morokuma, G.A. Voth, P. Salvadorm, J.J. Dannenberg, V.G. Zakrzewski, S. Dapprich, A.D. Daniels, M.C. Strain, O. Farkas, D.K. Malick, A.D. Rabuck, K. Raghavachari, J.B. Foresman, J.V. Ortiz, Q. Cui, A.G. Baboul, S. Clifford, J. Cioslowski, B. Stefanov, G. Liu, A. Liashenko, P. Piskorz, I. Komaromi, R.L. Martin, D.J. Fox, T. Keith, M.A. Al-Laham, C.Y. Peng, A. Nanayakkara, M. Challacombe, P.M.W. Gill, B. Johnson, W. Chen, M.W. Wong, C. Gonzalez, J.A. Pople, Gaussian 03, Revision C.02, Gaussian Inc., Wallingford, CT 06492, 2003.
[17] C.T. Lee, W.T. Yang, R.G. Parr, Phys. Rev. B 37 (1988) 785–789.
[18] R.G. Parr, W. Yang, Density Functional Theory of Atoms and Molecules, Oxford University Press, New York, 1989.
[19] A.D. Becke, J. Chem. Phys. 98 (1993) 5648–5652;
G.A. Petersson, A. Bennett, T.G. Tensfeldt, M.A. Allaham, W.A. Shirley, J. Mantzaris, J. Chem. Phys. 89 (1988) 2193–2218.
[20] C. Clavaguera-Sarrio, N. Ismail, C.J. Marsden, D. Begue, C. Pouchan, Chem. Phys. 302 (2004) 1–11.
[21] S.K. Adjokatse, A.K. Mishra, U.V. Waghmare, Polymer 53 (2012) 2751–2757.
[22] P. Pulay, G. Fogarasi, F. Pang, J.E. Boggs, J. Am. Chem. Soc. 101 (1979) 2550–2560.
[23] G. Fogarasi, X. Zhou, P.W. Taylor, P. Pulay, J. Am. Chem. Soc. 114 (1992) 8191–8201.
[24] J.M.L Martin, C. Van Alsenoy, Gar2ped, University of Antwerp, 1995.
[25] G.A. Zhurko, D.A. Zhurko, Chemcraft, 2005, <http://www.chemcraftprog.com>.
[26] M.D. Halls, J. Velkovski, H.B. Schlegel, Theor. Chem. Acc. 105 (2001) 413421.
[27] S. Mishra, P. Tandon, A.P. Ayala, Spectrochim. Acta Part A 88 (2012) 116–123.
[28] A.K. Mishra, P. Tandon, J. Phys. Chem. 113 (44) (2009) 14629–14639.
[29] C. Santhosh, P.C. Misra, J. Mol. Model. 3 (1997) 172–181.
[30] G.A. Guirgis, P. Klaboe, S. Shen, D.L. Powell, A. Gruodis, V. Aleksa, C.J. Nielsen, J. Tao, C. Zheng, J.R. Durig, J. Raman Spectrosc. 34 (2003) 322–336.
[31] P.L. Polavarapu, J. Phys. Chem. 94 (1990) 8106–8112.
[32] L.J. Bellamy, The Infrared Spectra of Complex Molecules, John Wiley, New York, 1956.
[33] G. Keresztury, Raman spectroscopy: theory, in: J.M. Chalmers, P.R. Griffiths (Eds.), Handbook of Vibrational Spectroscopy, vol. 1, John Wiley & Sons, New York, 2002.
[34] L.J. Bellamy, The IR spectra of Complex Molecules, John Wiley and Sons, New York, 1975.
[35] N.P.G. Roges, A Guide to the Complete Interpretation of the Infrared Spectra of Organic Structures, Wiley, New York, 1994.
[36] R.M. Silverstein, G.C. Bassler, T.C. Morrill, Spectrometric identification of organic compounds, third ed., John Wiley & Sons, New York, NY, 1974. p. 239.
[37] J. Mohan, Organic Spectroscopy-Principles Applications, Narosa Publishing House, New Delhi, 2001.